Article

Developmental Cell

TRANSPORTER OF IBA1 Links Auxin and Cytokinin to Influence Root Architecture

Graphical Abstract

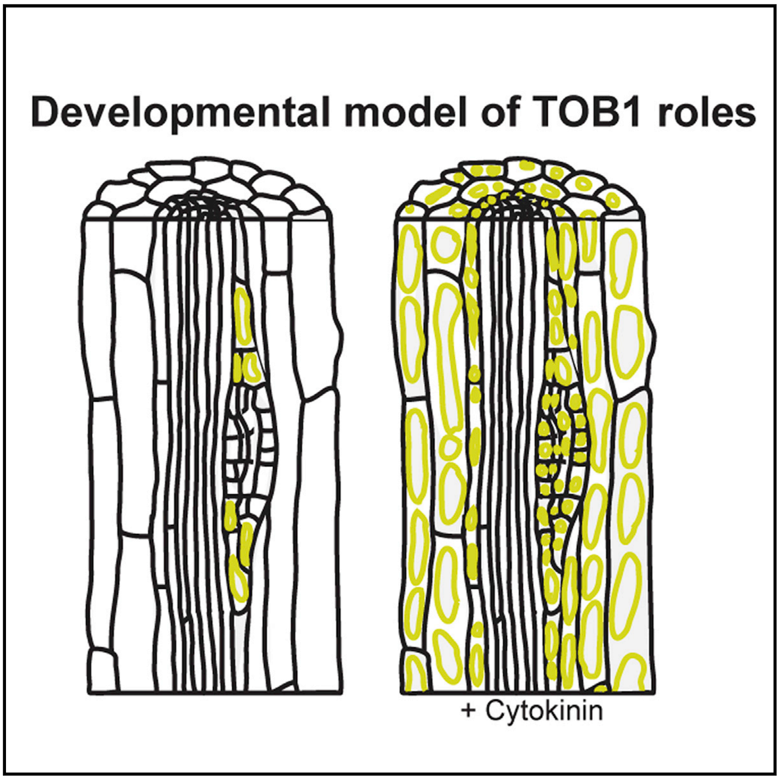

Authors

Marta Michniewicz, Cheng-Hsun Ho, Tara A. Enders, ..., Christopher N. Topp, Wolf B. Frommer, Lucia C. Strader

Correspondence

strader@wustl.edu

In Brief

Michniewicz and colleagues identify a vacuolar transporter of the auxin precursor indole-3-butyric acid (IBA) that regulates lateral root branching, which they named TOB1. *TOB1* is transcriptionally regulated by the phytohormone cytokinin to alter IBA contributions to the auxin pool, thus providing a mechanism for cytokinin to regulate lateral root development.

Highlights

- TRANSPORTER OF IBA1 (TOB1) identified as transporter of the auxin precursor IBA
- TOB1 localizes to the vacuolar membrane
- TOB1 regulates root system architecture (RSA)
- TOB1 integrates cytokinin response and auxin homeostasis to regulate RSA

Michniewicz et al., 2019, Developmental Cell *50*, 599–609
September 9, 2019 © 2019 Elsevier Inc.
https://doi.org/10.1016/j.devcel.2019.06.010

Developmental Cell
Article

TRANSPORTER OF IBA1 Links Auxin and Cytokinin to Influence Root Architecture

Marta Michniewicz,[1,7] Cheng-Hsun Ho,[2,3] Tara A. Enders,[1] Eric Floro,[4] Suresh Damodaran,[1] Lauren K. Gunther,[1] Samantha K. Powers,[1] Elizabeth M. Frick,[1] Christopher N. Topp,[4] Wolf B. Frommer,[2] and Lucia C. Strader[1,5,6,8,*]
[1]Department of Biology, Washington University, St. Louis, MO 63130, USA
[2]Institute for Molecular Physiology, Heinrich Heine Universität Düsseldorf, Institute for Biotransformative Molecules (WPI-ITbM), Nagoya University, Nagoya, Japan
[3]Agricultural Biotechnology Research Center, Academia Sinica, Taipei, Taiwan
[4]Donald Danforth Plant Science Center, St. Louis, MO 63132, USA
[5]Center for Engineering MechanoBiology, Washington University, St. Louis, MO 63130, USA
[6]Center for Science & Engineering of Living Systems, Washington University, St. Louis, MO 63130, USA
[7]Present address: Monsanto Company, 700 Chesterfield Parkway, Chesterfield, MO 63017, USA
[8]Lead Contact
*Correspondence: strader@wustl.edu
https://doi.org/10.1016/j.devcel.2019.06.010

SUMMARY

Developmental processes that control root system architecture are critical for soil exploration by plants, allowing for uptake of water and nutrients. Conversion of the auxin precursor indole-3-butyric acid (IBA) to active auxin (indole-3-acetic acid; IAA) modulates lateral root formation. However, mechanisms governing IBA-to-IAA conversion have yet to be elucidated. We identified TRANSPORTER OF IBA1 (TOB1) as a vacuolar IBA transporter that limits lateral root formation. Moreover, *TOB1*, which is transcriptionally regulated by the phytohormone cytokinin, is necessary for the ability of cytokinin to exert inhibitory effects on lateral root production. The increased production of lateral roots in *tob1* mutants, TOB1 transport of IBA into the vacuole, and cytokinin-regulated *TOB1* expression provide a mechanism linking cytokinin signaling and IBA contribution to the auxin pool to tune root system architecture.

INTRODUCTION

Plant root systems are critical for nutrient and water acquisition and also for anchoring the plant. Root system architecture is dynamically controlled and is altered in response to environmental conditions to allow for optimal plant growth (reviewed in Rogers and Benfey, 2015; Satbhai et al., 2015). In *Arabidopsis*, the primary root originates from the embryo and new meristems are initiated from cell divisions in the single-cell-layer pericycle along the root axis to generate lateral roots. During lateral root initiation, pericycle cells located at the xylem pole undergo several rounds of anticlinal cell divisions to produce a lateral root primordium. Subsequent rounds of division consist of both periclinal and anticlinal divisions to create a primordia that acquires similar tissue organization as the primary root, eventually emerging from the primary root as a fully patterned lateral root (reviewed in Lavenus et al., 2013).

Root system architecture, the spatial arrangement of roots in the root system, is an outcome of when and where lateral roots form, and by the angles and growth rates of each root. Architecture of a plant root system is dictated by both features inherent to the species and also to the soil conditions in which each plant finds itself. Proper root system architecture and dynamic response to soil conditions are necessary for successful plant growth.

The plant hormone auxin critically guides lateral root founder cell specification, initiation, and emergence (reviewed in Casimiro et al., 2003; Taylor-Teeples et al., 2016). Auxin activity in lateral root initiation is countered by cytokinin, which acts to suppress lateral root initiation (reviewed in Schaller et al., 2015). The balance of the activities of these two opposing hormones act to dynamically shape root system architecture.

Conversion of the auxin precursor indole-3-butyric acid (IBA) to the active auxin indole-3-acetic acid (IAA) is required for lateral root development (Strader et al., 2011; Zolman et al., 2008) and creates a local auxin source for the oscillating auxin-regulated gene expression that defines lateral root prebranch sites (De Rybel et al., 2012; Xuan et al., 2015). Despite the importance of IBA-to-IAA conversion during lateral root initiation, mechanisms governing IBA conversion are yet to be discovered. Here, we report the identification of an IBA carrier, which we have named TRANSPORTER OF IBA1 (TOB1) that likely acts to limit IBA contributions to the active auxin pool. Mutants defective in *TOB1* display increased numbers of lateral root primordia, emerged lateral roots, and accelerated growth rates. *TOB1* is expressed in the lateral root cap and also in specific cells surrounding lateral root primordia, suggesting that TOB1 acts in these cells to slow lateral root formation. Moreover, *TOB1* transcripts are upregulated by cytokinin and *tob1* mutants are resistant to the inhibitory effects of cytokinin on lateral root initiation, consistent with TOB1 acting as a mediator of cytokinin-auxin interactions in regulating lateral root formation.

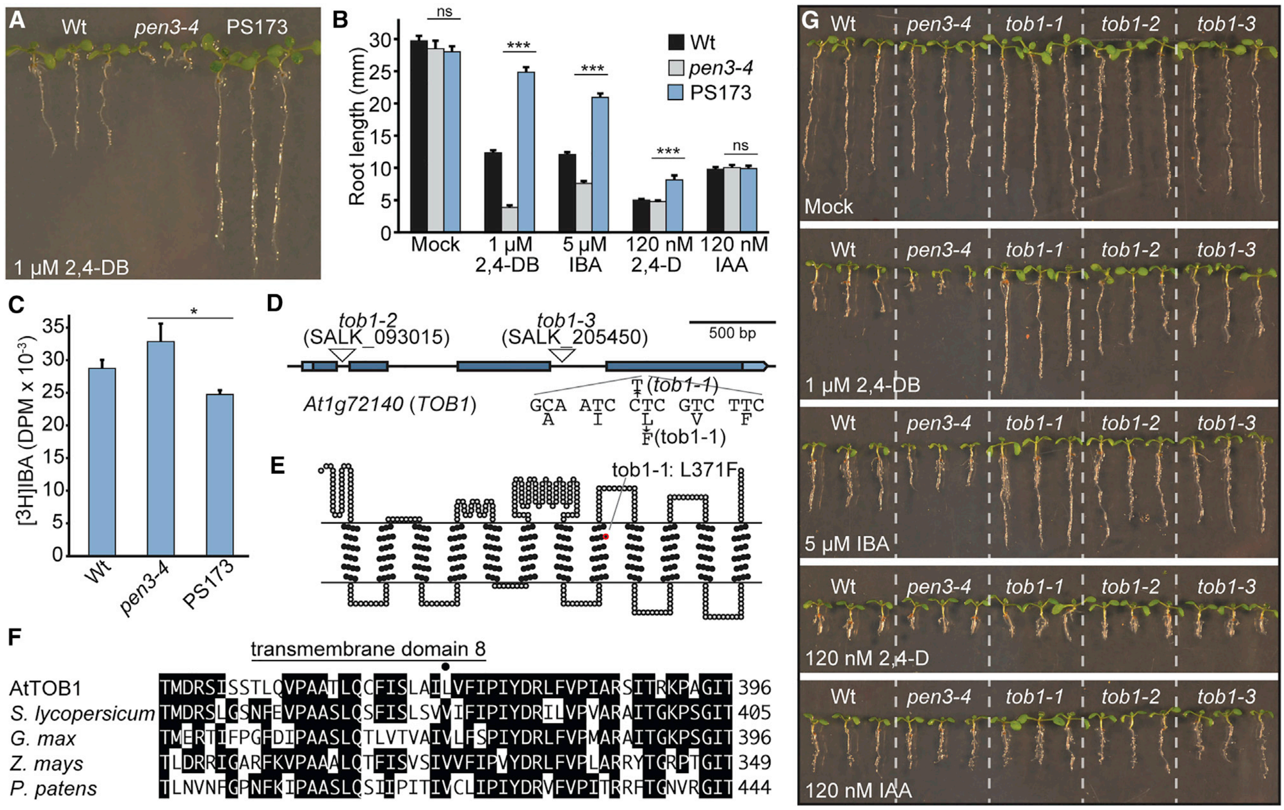

Figure 1. TRANSPORTER OF IBA1 Identification

(A) Photograph of 8-day-old WT (wild type) (Col-0), *pen3-4*, and PS173 (*pen3-4 tob1-1*) seedlings grown in the presence of 1 μM 2,4-DB.

(B) Mean primary root lengths (+SE; n ≥ 18) of 8-day-old WT (Col-0), PS173 (*pen3-4 tob1-1*), and *pen3-4* seedlings grown in the presence of the indicated auxins and auxin precursors. Statistical differences, as determined by a two-tailed t test assumming unequal variance, is indicated (***p ≤ 0.001; ns, no significant difference observed).

(C) Root tips of WT (Col-0), *pen3-4*, and PS173 (*pen3-4 tob1-1*) seedlings were incubated for 1 h in uptake buffer containing 25 nM [^{3}H]-IBA, rinsed three times with uptake buffer, and then removed and analyzed by scintillation counting. Mean DPM (+SE; n = 6) are shown. Statistical differences, as determined by a two-tailed t test assumming unequal variance, is indicated (*p ≤ 0.05).

(D) *TOB1/At1g72140* gene schematic depicting the EMS-consistent point mutation identified in PS173 (called *tob1-1*) and two T-DNA insertion alleles (*tob1-2* and *tob1-3*).

(E) A schematic diagram of the predicted TOB1 topology based on outputs of ARAMEMNON (http://aramemnon.uni-koeln.de; Schwacke et al., 2003) and TOPO2 (http://www.sacs.ucsf.edu/TOPO2/). Filled circles represent predicted transmembrane residues whereas open circles represent non-transmembrane residues. *tob1-1* carries a Leu371-to-Phe substitution in the eighth predicted transmembrane domain.

(F) The *tob1-1* mutation disrupts a conserved aliphatic residue in the eighth predicted transmembrane domain. The alignment shows this region in *Arabidopsis thaliana* TOB1 (At1g72140) and its closest homologs from *Solanum lycopersicum*, *Glycine max*, *Zea mays*, and *Physcomitrella patens*.

(G) Photographs of representative 8-day-old WT (Col-0), *pen3-4*, *tob1-1*, *tob1-2*, and *tob1-3* seedlings grown in the presence of the indicated auxins.

RESULTS

Identifying TRANSPORTER OF IBA1

Conversion of the auxin precursor indole-3-butyric acid (IBA) contributes to the auxin pool to drive multiple developmental events, including lateral root development (reviewed in Strader and Bartel, 2011). Despite the significance of IBA contributions to auxin-regulated developmental processes, mechanisms to regulate IBA inputs to the auxin pool have not been identified. We used a forward genetics approach to identify factors that may act to modulate IBA levels.

Mutants defective in *ABCG36/PDR8/PEN3* (Strader and Bartel, 2009) display hypersensitivity to the auxin precursor IBA, but not to the active auxin indole-3-acetic acid (IAA), likely because of a defect in efflux of this auxin precursor from root cells (reviewed in Michniewicz et al., 2014). In addition, *abcg36* mutants hyperaccumulate [^{3}H]-IBA in simplified auxin transport assays (Strader and Bartel, 2009), consistent with a defect in efflux of this molecule. To identify additional IBA transporters, we performed a suppressor screen of the *pen3-4* allele of *ABCG36* (Figure S1A). Isolate PS173 from this screen displayed suppression of *pen3-4* hypersensitivity to both IBA and to its synthetic analog 2,4-dichlorophenoxy butyric acid (2,4-DB; Figures 1A and 1B). Isolate PS173 also displayed suppression of *pen3-4* hyperaccumulation of [^{3}H]-IBA (Figure 1C). Using whole genome sequencing combined with bulk segregant analysis (Thole and Strader, 2015), we identified three homozygous EMS-related mutations in PS173 (Figure S1C). One of these was a missense mutation in *At1g72140*, encoding the Major Facilitator Superfamily (MFS) member NPF5.12 (Figure 1D),

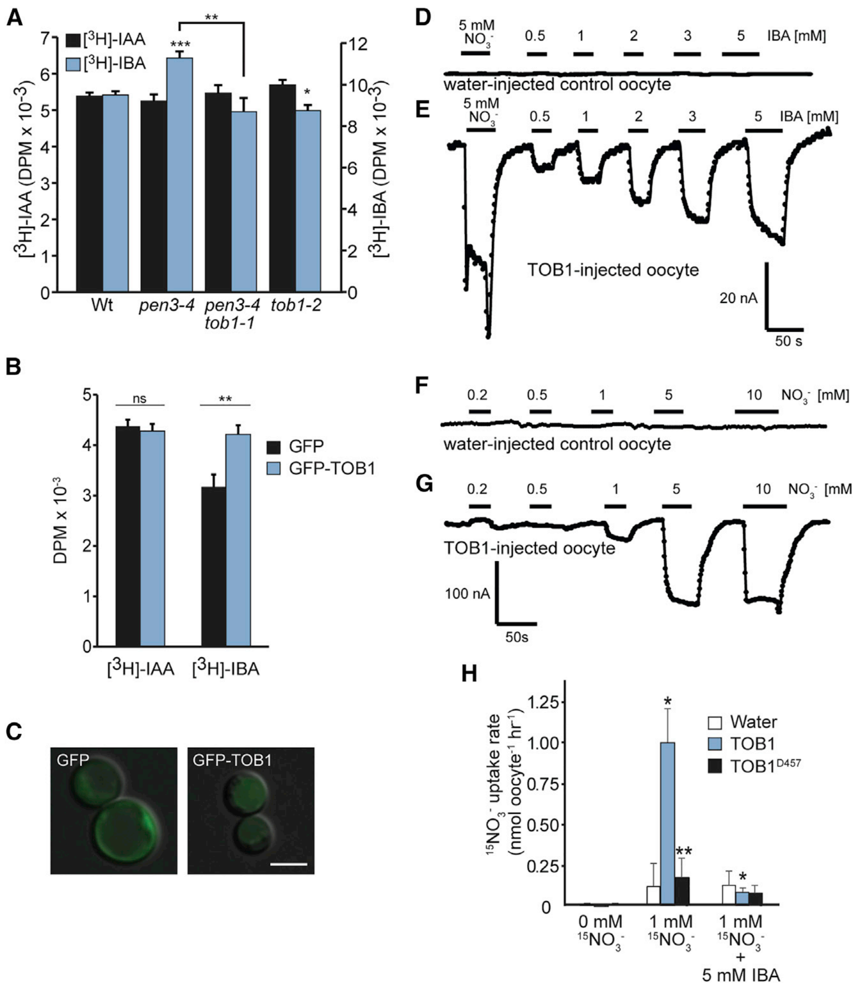

Figure 2. TOB1 Transports the Auxin Precursor IBA

(A) Root tips of WT (Col-0), *pen3-4*, PS173 (*pen3-4 tob1-1*), and *tob1-2* seedlings were incubated for 1 h in uptake buffer containing 25 nM [^{3}H]-IAA or 25 nM [^{3}H]-IBA, rinsed three times with uptake buffer, and then removed and analyzed by scintillation counting. Mean DPM (+SE; n = 6) are shown. Statistical differences, as determined by a two-tailed t test assumming unequal variance, is indicated (***p $\leq$ 0.001; **p $\leq$ 0.01; *, p $\leq$ 0.05; ns, no significant difference observed).

(B) *Saccharomyces cerevisiae* strain BY4741 carrying pAG424-GFP or pAG424-GFP-TOB1 were incubated for 1 h in buffer containing 25 nM [^{3}H]-IAA or 25 nM [^{3}H]-IBA, rinsed three times with buffer, and then analyzed by scintillation counting. Mean DPMs (+SE; n = 12) are shown. Statistical differences, as determined by a two-tailed t test assumming unequal variance, is indicated (**p $\leq$ 0.01; ns, no significant difference observed).

(C) GFP-TOB1 is primarily localized to the vacuolar membrane in yeast cells. Fluorescence microscopy images of *Saccharomyces cerevisiae* strain BY4741 carrying pAG424-GFP or pAG424-GFP-TOB1. Scale bar, 5 μm.

(D and E) Representative currents recorded in single oocytes injected with water as a control (D) or *TOB1* (E) when perfused with IBA or nitrate at indicated concentrations (independent data from three different oocytes from three different frogs were recorded). Oocytes were clamped at −120 mV.

(F and G) Representative currents recorded in single oocytes injected with water (F) or *TOB1* (G) when perfused with nitrate at the various indicated concentrations (independent data from three different oocytes from three different frogs were recorded). Oocytes were clamped at −120 mV.

(H) Mean (±SD; n $\geq$ 5) $^{15}NO_3^-$ uptake in water-, *TOB1*-, and *TOB1^{D457A}*-injected oocytes incubated with 1 mM $K^{15}NO_3$ buffer (pH 5.5) with or without 5 mM IBA for 1 h. Asterisks indicate significant differences (p $\leq$ 0.05, t test).

resulting in a Leu371-to-Phe substitution in transmembrane domain 8 (Figures 1E and 1F). We obtained insertional alleles defective in *At1g72140* (Figure 1D) and found that these, like our missense allele, displayed mild resistance to the long-chain auxins IBA and 2,4-DB and wild-type sensitivity to the active auxins IAA and 2,4-D (Figure 1G), consistent with the possibility that the defect in *At1g72140* causes *pen3-4* suppression in isolate PS173. Because these insertional alleles displayed similar phenotypes as the missense allele in *At1g72140* removed from the *pen3-4* background (Figure 1G), we named this gene *TRANSPORTER OF IBA1* (*TOB1*). We named the original missense allele *tob1-1* and the insertional alleles *tob1-2* (SALK_093015) and *tob1-3* (SALK_205450; Figure 1D).

TOB1 Transports IBA

The mildly decreased IBA responsiveness of the *tob1* alleles (Figure 1G) combined with the identity of TOB1 as a member of the MFS transporter family (reviewed in Léran et al., 2014), suggested that TOB1 might function in IBA transport. To test this possibility, we examined [^{3}H]-IAA and [^{3}H]-IBA accumulation in *tob1* alleles using an excised root tip auxin transport assay (Ito and Gray, 2006; Strader and Bartel, 2009; Strader et al., 2008). Consistent with the wild-type sensitivity of these alleles to IAA in root elongation assays (Figure 1G), *tob1* alleles displayed wild-type [^{3}H]-IAA accumulation in this assay (Figure 2A). However, *tob1* root tips accumulated less [^{3}H]-IBA than did wild-type root tips in this assay (Figure 2A). Moreover, *tob1* fully suppressed the increased accumulation of [^{3}H]-IBA observed in *pen3-4* root tips (Figure 2A). These results suggest that TOB1 is necessary for IBA transport in plants.

To determine whether TOB1 directly transports IBA, we expressed either free GFP or GFP-TOB1 in *Saccharomyces cerevisiae* and examined accumulation of [^{3}H]-IAA and [^{3}H]-IBA. Whereas [^{3}H]-IAA accumulation was similar in both strains, GFP-TOB1-expressing yeast accumulated more [^{3}H]-IBA than yeast expressing free GFP (Figure 2B), consistent with direct IBA transport by TOB1 in this heterologous system. Examination of GFP-TOB1 revealed that it primarily localizes to the vacuolar membrane in yeast (Figure 2C); however, we cannot exclude the possibility that a small amount of GFP-TOB1 localizes to the

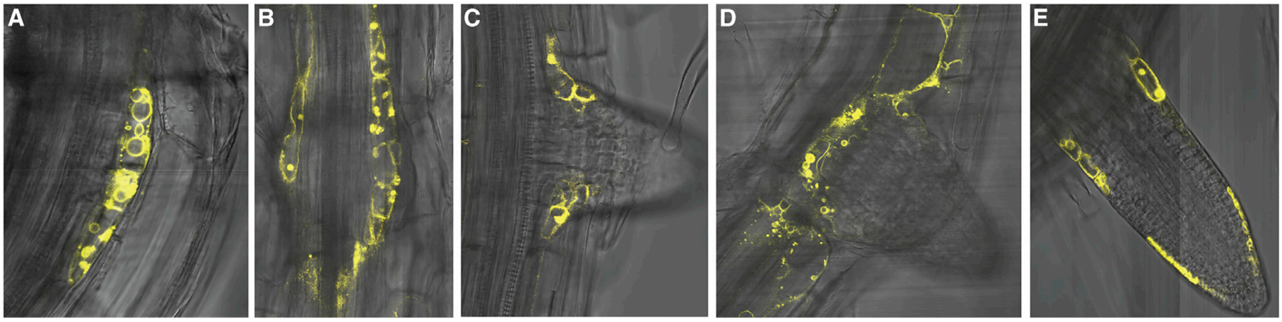

Figure 3. Vacuolar TOB1 Accumulates in Lateral Root Cap and Lateral Root Primordia Cells

TOB1 is expressed during all stages of lateral root development. Confocal microscopy images from *tob1-1*expressing *TOB1:YFP-TOB1*, imaging lateral roots (A) at early lateral root initiation, (B) a top-down view of a developing lateral root (C) a side view of a developing lateral root, (D) after emergence, (E) the developing lateral root tip.

plasma membrane to drive IBA accumulation. The hyperaccumulation of [^{3}H]-IBA in GFP-TOB1-expressing yeast along with its localization to the vacuolar membrane is consistent with TOB1 moving IBA from the cytoplasm and into the vacuole of yeast cells.

We further examined the ability of *TOB1* expressed in *Xenopus* oocytes to transport IBA. Two-electrode voltage clamp analysis revealed that IBA induced concentration-dependent currents ($K_m \sim$2.7 mM; Figures 2D–2G and S2), consistent with IBA transport by TOB1. Because TOB1/NPF5.12 is a member of a transporter family with members that transport nitrate, we also examined nitrate transport by two-electrode voltage clamp analysis and found that, similar to a previous report (He et al., 2017), nitrate-induced concentration-dependent currents ($K_m \sim$1.7 mM; Figures 2D–2G, S2A, and S2B). In both cases, currents were pH dependent and higher at acidic versus neutral pH (Figure S2D). Nitrate currents were significantly larger than IBA currents (Figures 2D–2G and S2E–S2G). Nitrate uptake was confirmed by isotope uptake assays; IBA competed for nitrate uptake (Figure 2H). Other hormones such as ABA, GA_3, GA_4, and IAA, which are transported by other members of the CHL1/PTR/NPF family, do not induce substantial currents, intimating that TOB1 is specific for IBA and nitrate (Figures S2H–S2J). To exclude that currents were caused by induction of oocyte endogenous channels, a non-functional TOB1 mutant was generated. D547 in TOB1 corresponds to the essential E476 glutamate in CHL1 (Ho and Frommer, 2014). The D547A mutant of TOB1 lost both IBA and nitrate-induced currents (Figures 2H, S2K, and S2L). In addition to IBA and nitrate-induced inward currents, we also observed a chloride-dependent outward current (Figure S2M). Taken together, these data indicate that, in *Xenopus* oocytes, TOB1 mediates uptake of the IBA and nitrate anions, likely together with two protons, similar to other members of the family (Zhou et al., 1998). In addition, it is conceivable that the transporter has a chloride conductance as has been observed for NPF2.4, a TOB1 paralog (Li et al., 2016). The ability of heterologously expressed TOB1 to transport IBA implies a direct role for TOB1 in transporting this auxin precursor.

Tonoplast-Localized TOB1 Represses Lateral Root Development

To examine TOB1 localization and function, we transformed the *tob1-1* mutant with a construct carrying a TOB1-promoter driven YFP-TOB1 fusion protein (*TOB1:YFP-TOB1*), which rescued the *tob1-1* mutant phenotype (Figures S3A and S3B). We found that YFP-TOB1 co-localized with a tonoplast marker (Figures S3C and S3D), similar to a previous report that NPF5.12-EYFP localized to the tonoplast when expressed in *Arabidopsis* mesophyll protoplasts (He et al., 2017), although we cannot exclude the possibility that a small amount of TOB1 may localize to other membranes. Vacuolar YFP-TOB1 signal accumulated in lateral root cap cells in the primary root tip (Figure S3E) and in lateral root associated cells during all examined stages of lateral root development (Figures 3A–3E). We detected YFP-TOB1 signal in the first dividing cells of the lateral root primordia (Figure 3A). As additional cell divisions occurred during lateral root primordia development, YFP-TOB1 signal became restricted to the pericycle cells surrounding the primordia (Figure 3B) and to the basal margins of the lateral root primordia (Figures 3C and 3D). After the lateral root emerged and developed an organized meristem, YFP-TOB1 signal was also detected in the lateral root cap cells of the new lateral root (Figures 3E and S3E). Because the *TOB1:YFP-TOB1* construct complemented the *tob1-1* phenotype (Figures S3A and S3B), the YFP-TOB1 vacuolar localization in lateral root-associated tissues likely reflects functional TOB1 sites.

We found that *TOB1* is expressed in lateral root cap cells (Figures 3E and S3E), a site in which oscillations of IBA-to-IAA conversion are important for positioning the priming sites in lateral root initiation (De Rybel et al., 2012; Xuan et al., 2015), and also in cells associated with lateral root primordia (Figures 3C–3G). We therefore examined lateral root development in *tob1* mutants and discovered that these mutants display increased lateral root density and longer lateral roots (Figure 4A). An analysis of pre-emerged lateral roots revealed an increased density of lateral root initials in *tob1-2* after 4 days and 8 days of growth, which resulted in an increased density of emerged lateral roots in 8-day-old seedlings (Figure 4B).

The longer lateral roots observed in *tob1* raised the possibility that lateral root development progressed more quickly in *tob1* than in wild type. To assess this possibility, we used gravitropic stimulation to synchronize lateral root primorida initiation in 6-day-old wild-type and *tob1-2* seedlings carrying the *DR5-GFP* reporter (Friml et al., 2003). Gravitropic stimulation of lateral root primordia initiation typically results in one lateral root

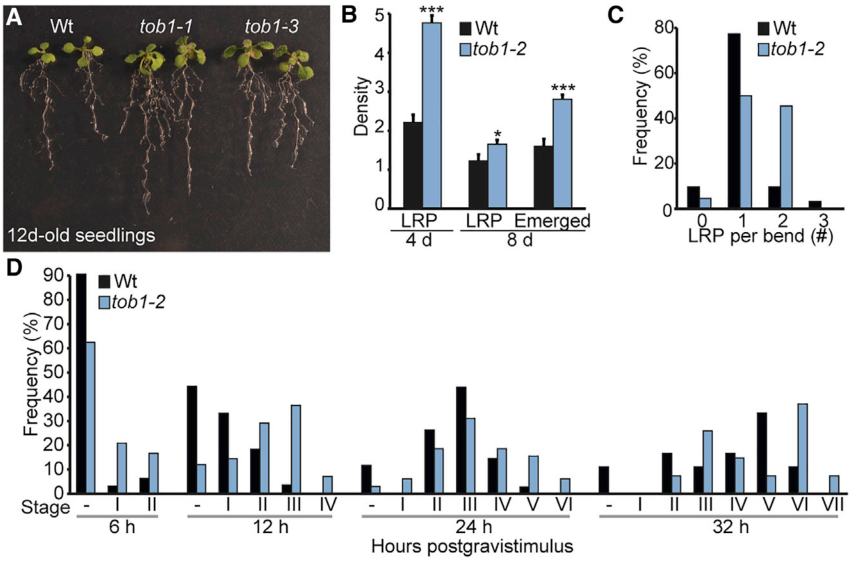

Figure 4. TOB1 Regulates Lateral Root Formation

(A) *tob1* mutant seedlings display increased numbers of lateral roots and longer lateral roots than wild type. Photograph of 12-day-old WT (Col-0), *tob1-1*, and *tob1-3* seedlings.

(B) Unemerged lateral root primordia (LRP) and emerged lateral roots were quantified in WT (Col-0) and *tob1-2* seedlings carrying the *DR5-GFP* reporter (Friml et al., 2003) after 4 or 8 days of growth. Lateral root density was measured as number of lateral roots per cm primary root length (mean + SE; n $\geq$ 26). Statistical differences, as determined by a two-tailed t test assumuning unequal variance, is indicated (***p $\leq$ 0.001; *p $\leq$ 0.05).

(C) Gravitropic stimulation was used to synchronize lateral root initiation in 6-day-old WT (Col-0) and *tob1-2* seedlings carrying the *DR5-GFP* reporter (Friml et al., 2003). Histogram of frequency of lateral root primordia per root bend after 24 h of gravistimulus. *tob1-2* number of lateral roots per bend was significantly different from wild type (two-tailed t test assumuning unequal variance, p $\leq$ 0.05).

(D) Gravitropic stimulation was used to synchronize lateral root primorida initiation in 6-day-old WT (Col-0) and *tob1-2* seedlings carrying the *DR5-GFP* reporter (Friml et al., 2003). After 6, 12, 24, and 32 h of gravistimulus, lateral root stages (Malamy and Benfey, 1997) of primordia at the induced root bend were determined. Histograms depict frequency of lateral root stages observed at these time points (n $\geq$ 30).

primordia per root bend. Consistent with the increased lateral root initial density observed in *tob1-2* (Figure 4B), we found that *tob1-2* produced two lateral root primordia per gravitropic bend more frequently than wild type (Figure 4C). At each of the post-gravistimulus time points observed, lateral root primordia in *tob1-2* were more developed than those in wild type (Figure 4D), consistent with a role for TOB1 in slowing progression of lateral root primordia development.

The *tob1* phenotype of increased lateral root production (Figure 4), combined with the TOB1 identity as a tonoplast-localized (Figure 3A) transporter of the auxin precursor IBA (Figure 2), suggests a role for TOB1 in limiting IBA contributions to auxin homeostasis. Thus, in the absence of TOB1, IBA contributions to the auxin pool may be increased in certain cells resulting in increased auxin-driven lateral root initiation and growth. This phenotype is converse to the decreased lateral root phenotype found in the IBA conversion mutant *ech2 ibr10* (Strader et al., 2011; Zolman et al., 2008). We therefore examined the triple mutant and found that blocking IBA conversion suppressed the increased lateral root phenotype displayed by *tob1*, suggesting that IBA conversion acts downstream of TOB1 effects on lateral root development. Because models suggest IBA-to-IAA conversion in the lateral root cap could contribute to root cap sloughing associated with lateral root priming (Xuan et al., 2016), we examined root cap sloughing in *tob1* alleles, finding no differences with wild type under the tested conditions (Figure S4).

Whereas the essential effects of *tob1* mutations on seedling root growth could be assessed with plate-based assays, the consequences for three-dimensional architecture during plant development required a different approach. We quantified the growth of each root (primary and all laterals) from day 9 to day 25 (bolting) using a gel-based 3D root imaging and analysis pipeline (Symonova et al., 2015; Topp et al., 2013). Consistent with the seedling plate assays, *tob1-1* had more roots and a greater total root length than wild type at each of the five timepoints (Figures 5B–5D, 5F, 5K, and 5L). However, the primary root lengths of mutant and wild type were indistinguishable (Figure 5B), as were the volumes of space that the root systems explored (convex hull volume; Figure 5N). Thus, if there are more roots within a similar volume in *tob1-1* mutants, then the thoroughness of exploration of that space is greater, a trait with significant implications for root foraging in natural environments that can apparently be selected for as a function of natural history (Topp et al., 2013). Our time series analysis also allowed us a view on growth patterns, notably that lateral roots of *tob1-1* mutants grew more rapidly at early stages of development (Figure 4D; 5H), but elongation rates were then eclipsed by wild type by day 13. These results can be interpreted in terms of a rhizoeconomic theory (Lynch et al., 2005) in which a finite amount of carbon is apportioned to root growth, for example, either to generate new roots (*tob1* > wild type), or to continue elongation of existing roots > *tob1*). In sum these results reinforce a role of TOB1 to moderate the emergence and early elongation of lateral roots, which can affect the foraging patterns of the plant. Additionally, they highlight the importance of time-resolved phenotype measurements, because the elongation rate increase in *tob1-1* mutants is eventually lost, perhaps due to plant physiological processes not directly related to TOB1 function, such as carbon or nutrient limitations on growth.

TOB1 Is Regulated by Cytokinin

Cross-regulation between auxin and cytokinin regulates lateral root development (reviewed in Chandler and Werr, 2015; Schaller et al., 2015). Similar to the apparent TOB1 role in limiting lateral root development, the plant hormone cytokinin inhibits lateral root development. We therefore examined *tob1* responsiveness to cytokinin and *TOB1* regulation by cytokinin. We found that *tob1* mutants displayed wild-type responsiveness to inhibition

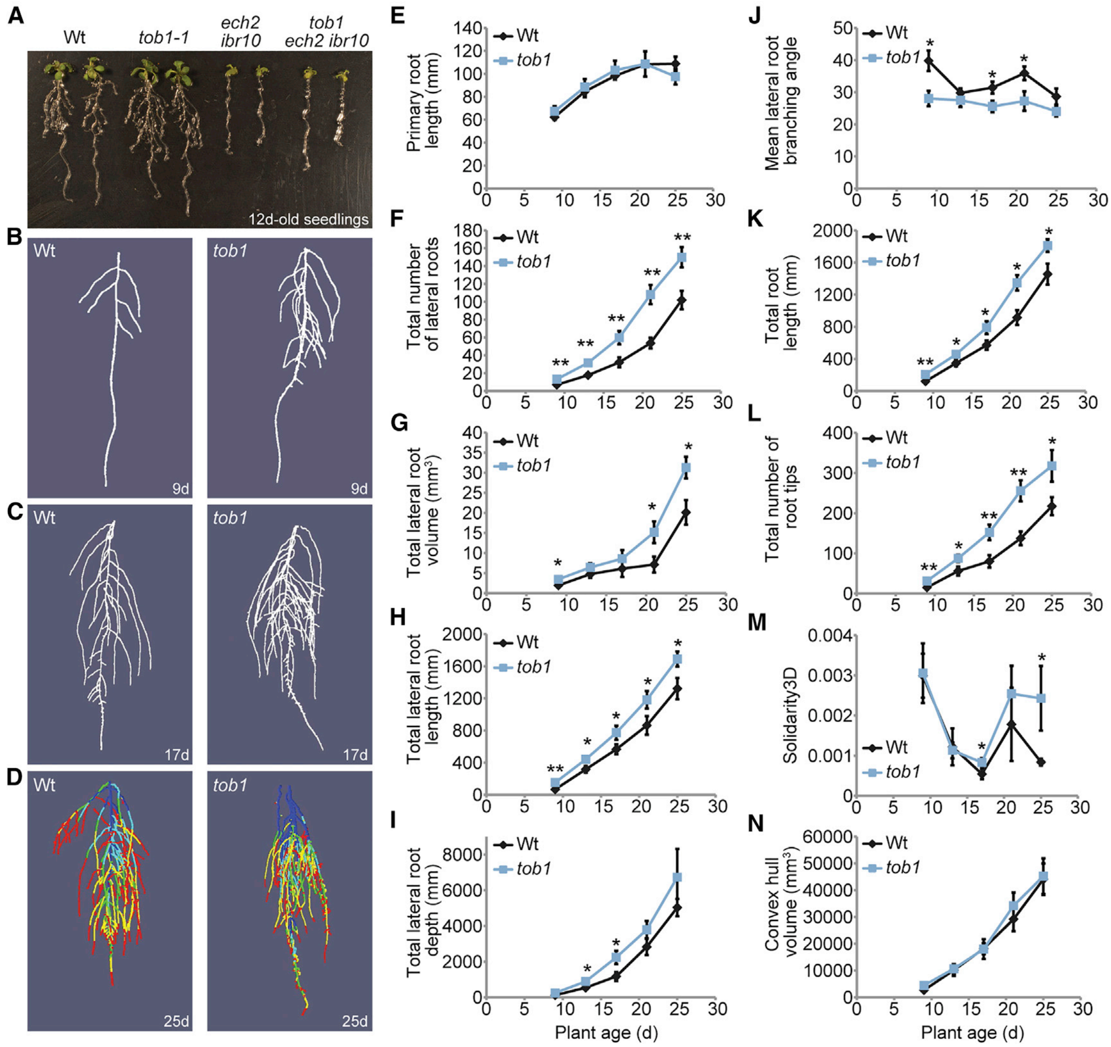

Figure 5. TOB1 Regulates Root System Architecture

(A) *tob1* lateral root phenotypes are suppressed by blocking IBA-to-IAA conversion. Photograph of 12-day-old WT (Col-0), *tob1-1*, *ech2-1 ibr10-1*, and *tob1-1 ech2-1 ibr10-1* seedlings.

(B–D) Selected 2D projections of 3D reconstructions of 9-day-old (B), 17-day-old (C), or 25-day-old (D) Wt (Col-0) and *tob1-1* plants. Growth since the last time point is indicated by progressively warmer colors (D). Videos S1, S2, S3, and S4 convey 3D views.

(E–J) Root traits obtained from 3D reconstructions of WT (Col-0) and *tob1-1* plants after 9, 13, 17, 21, or 25 days of growth using Dynamic Roots software, which parses each root in the system for measurements over time (Symonova et al., 2015). See Data S1 for full dataset. WT and *tob1* display no observable difference in primary root length (E). Compared to Wt, *tob1* displays increased total number of lateral roots (F), total lateral root volume (G), total lateral root length (H), and total lateral root depth (I) at certain time points. *tob1* displays a decreased mean lateral root branching angle compared to WT at certain time points (J). Asterisk indicates significant difference (*$p \leq 0.05$, **$p \leq 0.01$; non-parametric Wilcoxon 2-sample test with normal approximation).

(K–N) Root traits obtained from 3D reconstructions of WT (Col-0) and *tob1-1* plants after 9, 13, 17, 21, or 25 days of growth using the RSA-GIA pipeline, which captures global features of root systems (Galkovskyi et al., 2012; Topp et al., 2013). See Data S2 for full dataset. *tob1-1* displays increased total root length (K), increased total number of root tips (L), and increased solidity (the thoroughness with which a root system explores a volume of soil; (M) at certain time points. The convex hull volumes of WT and *tob1-1* were indistinguishable at the examined time points. Asterisk indicates significant difference (*$p \leq 0.05$, **$p \leq 0.01$; non-parametric Wilcoxon two-sample test with normal approximation).

of root elongation by cytokinin (Figure 6A) but displayed resistance to inhibition of lateral root formation by cytokinin (Figure 6B), suggesting a specific role for TOB1 in mediating repression of lateral root formation by cytokinin. *TOB1* transcript accumulation was upregulated by a one-h cytokinin treatment (Figure 6C). In addition, *TOB1* transcript levels were lower than wild-type levels in the *ahk3 ahk4* mutant (Nishimura et al., 2004), defective in two cytokinin receptors (Figure 6C). Conversely, *TOB1* accumulation was elevated in the *arr3,4,5,6,7,8,9,15* octuple mutant (Zhang et al., 2011), defective in eight type A-ARABIDOPSIS RESPONSE REGULATORs (ARRs) that repress cytokinin responses (Figure 6C). Promotion of *TOB1* levels by cytokinin treatment combined with its altered accumulation in cytokinin response mutants suggests that *TOB1* transcripts are under the control of the

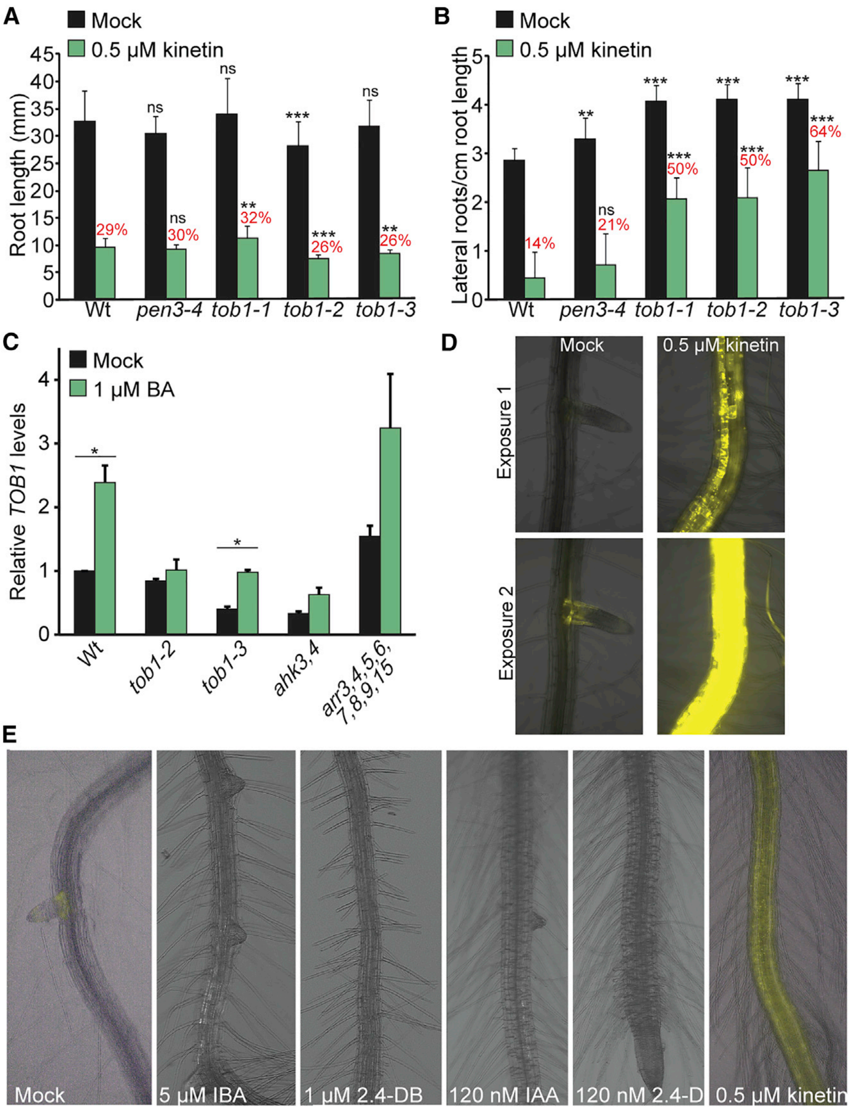

Figure 6. Cytokinin Regulates *TOB1* Expression

(A) Mean primary root lengths (+SD; n $\geq$ 11) of 10-day-old WT (Col-0), *pen3-4*, *tob1-1*, *tob1-2*, and *tob1-3* seedlings grown on medium supplemented with ethanol (Mock) or 0.5 µM kinetin. Percent inhibition by treatment is indicated above each treatment bar. Statistical differences, as determined by a two-tailed t test assumuning unequal variance, is indicated (***p $\leq$ 0.001; **p $\leq$ 0.01; ns, no significant difference observed).

(B) Mean numbers of lateral roots per cm of root length (+SD; n $\geq$ 11) of 10-day-old WT (Col-0), *pen3-4*, *tob1-1*, *tob1-2*, and *tob1-3* seedlings grown on medium supplemented with ethanol (Mock) or 0.5 µM kinetin. Percent inhibition by treatment is indicated above each treatment bar. Statistical differences, as determined by a two-tailed t test assumuning unequal variance, is indicated (***p $\leq$ 0.001; **p $\leq$ 0.01; ns, no significant difference observed).

(C) *TOB1* transcript is cytokinin-regulated. 6-day-old WT (Col-0), *tob1-2*, *tob1-3*, *ahk3-1 ahk4-1* (Nishimura et al., 2004), and *arr3 arr4 arr5 arr6 arr7 arr8 arr9 arr15* (Zhang et al., 2011) seedlings were incubated for 1 h in medium supplemented with ethanol (Mock) or 1 µM BA. Relative *TOB1* transcript levels (mean of three biological replicates, each with three technical replicates; +SE) were determined using quantitative PCR using cDNA from each sample. *TOB1* transcript levels under mock conditions and under BA-treated conditions were significantly different from wild type for *tob1-2*, *tob1-3*, and *ahk3,4* ($p < 0.05$, t test assuming unequal variance). Asterisks indicate a significant difference ($p < 0.05$, t test assuming unequal variance) between mock and BA-treated samples for individual genotypes.
Statistical differences, as determined by a two-tailed t test assumuning unequal variance, is indicated (***p $\leq$ 0.001; **p $\leq$ 0.01; *p $\leq$ 0.05; ns, no significant difference observed).

(D) Cytokinin upregulates TOB1 levels in all root tissues. Confocal images of 6-day-old *tob1-1 TOB1:YFP-TOB1* grown on medium supplemented with ethanol (Mock) or 0.5 µM kinetin. Two exposures for each condition are shown.

(E) Fluorescence microscopy images of 6-day-old *tob1-1 TOB1:YFP-TOB1* grown on medium supplemented with ethanol (Mock) or the indicated hormone are shown.

cytokinin signaling system. Consistent with this possibility, two ARR binding sequences, consisting of A(A/G)GAT(T/C)TT (core sequences underlined), lie upstream of the *TOB1* transcript initiation site, three ARR binding sequences are found within the second *TOB1* intron and five ARR binding sequences are immediately downstream of the *TOB1* stop codon (Figure S5), and ARR10 may directly bind the *TOB1* promoter (Zubo et al., 2017).

Although *TOB1:YFP-TOB1* signal is typically limited to specific root cell types (Figure 3), we found that growing seedlings in the presence of cytokinin dramatically increased YFP-TOB1 signal and expanded the signal to all examined root cell types (Figures 6D and 6E). In contrast, growth in the presence of various auxins did not increase *TOB1:YFP-TOB1* signal (Figure 6E). The TOB1 requirement for cytokinin inhibition of lateral root formation combined with *TOB1* transcriptional control by the cytokinin signaling system suggests a model in which cytokinin upregulates *TOB1*, resulting in limited IBA contributions to the auxin pool and thus limited lateral root formation (Figure 7).

DISCUSSION

Auxin - cytokinin cross-regulation controls multiple developmental events, including lateral root development (reviewed in Chandler and Werr, 2015; Schaller et al., 2015). Whereas auxin promotes lateral root initiation and development, cytokinin has an inhibitory role in lateral root organogenesis. Our identification of TOB1 as a mediator of the interactions between cytokinin and auxin in lateral root development adds to a growing body of mechanisms regulating this process. Auxin promotes new lateral root primordia (reviewed in Casimiro et al., 2003; Taylor-Teeples

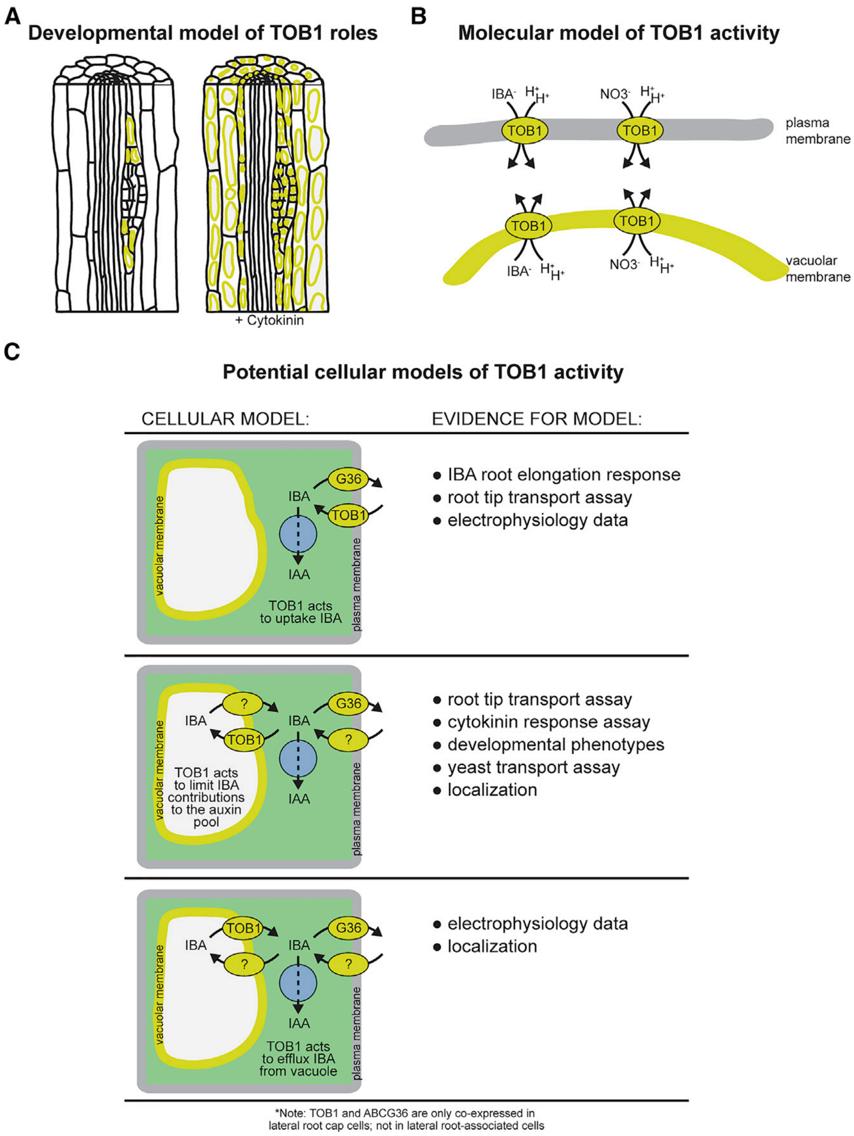

Figure 7. Model of TOB1 Activity

(A) Developmental model of TOB1 activity. The *TOB1* gene is a direct target of the cytokinin response pathway and mediates cytokinin effects on lateral root development. Loss of TOB1 activity results in increased numbers of emerged lateral roots.

(B) Molecular model of TOB1 activity. Electrophysiology experiments suggest that TOB1 transports IBA, along with two protons, across the occyte plasma membrane into the cytoplasm. The directionality of this transport is consistent with TOB1-mediated efflux of IBA from the vacuole.

(C) Potential cellular models of TOB1/NPF5.12 activity. Three potential models for TOB1 activity within the cell; each are differentially supported by the data. A model in which plasma-membrane-localized TOB1 acts to uptake IBA is supported by our IBA-responsive root elongation data, our root tip IBA transport assay, and our electrophysiology data in oocytes. A model in which tonoplast-localized TOB1 transports IBA and nitrate to affect lateral root production by sequestering these molecules is supported by our root tip IBA transport assay, our cytokinin response assay, the *tob1* developmental phenotypes, our yeast transport assay, and YFP-TOB1 localization. A model in which tonoplast-localized TOB1 transports IBA out of the vacuole is supported by YFP-TOB1 localization and electrophysiology data in oocytes. Our conflicting data for TOB1 cellular activity suggest that additional factors regulating TOB1 localization or activity are missing.

et al., 2016) and auxin response oscillations at the root tip specify sites of future lateral root primordia (De Smet et al., 2007; Moreno-Risueno et al., 2010). Mutants defective in cytokinin responsiveness or cytokinin accumulation display increased numbers of lateral roots compared to wild type (reviewed in Schaller et al., 2015). Because cytokinin response regulates lateral root density (Bielach et al., 2012; Chang et al., 2013), cytokinin is thought to regulate the auxin-mediated oscillation pattern setting the lateral root spacing. During later stages of lateral root development, cytokinin promotes targeting of the PIN1 auxin (IAA) efflux carrier to vacuoles for lytic degradation (Marhavý et al., 2011) and altered cytokinin response leads to altered PIN1 localization (Laplaze et al., 2007; Marhavý et al., 2011, 2014; Moreira et al., 2013). Cytokinin Response factors, cytokinin-inducible transcription factors, directly bind PIN1 and PIN7 upstream regulatory regions and cytokinin treatment increases expression of these genes encoding auxin efflux carriers (Šimášková et al., 2015). Our developmental model (Figure 7A) suggests that TOB1 transports the auxin precursor IBA into the vacuole to limit IBA contributions to the auxin pool and also mediates cytokinin effects on lateral root formation. Mutants defective in *TOB1* are resistant to the inhibitory effects of cytokinin on lateral root formation (Figure 5B), and *TOB1* transcript accumulation is regulated by cytokinin (Figures 5C–5E), providing an additional mechanism through which cytokinin exerts its effects on auxin homeostasis to direct lateral root formation (Figure 6). Together, the activities of the critical plant hormones auxin and cytokinin drive lateral root specification and activation to ultimately affect the architecture of the root system.

TOB1 is a member of a family of transporters classified as the NTR1 PTR Family (NPF) (Léran et al., 2014), which are a part of the larger group of MFS transporters. MFS transporters are a large and diverse family of secondary transporters with substrates including ions, sugars, amino acids, and peptides. Members of the NPY/NRT1/CHL1 family, originally identified as nitrate and peptide transporters (Frommer et al., 1994; Rentsch et al., 1995; Tsay et al., 1993), also transport many key plant hormones. CHL1, the dual affinity nitrate transceptor, appears to also transport IAA (Krouk et al., 2010; Mounier et al., 2014); other members of this large family transport compounds as diverse as chloride, abscisic acid, gibberellin, JA-Ile, and glucosinolates (Chiba et al., 2015; Kanno et al., 2012; Li et al., 2016; Nour-Eldin et al., 2012; Saito et al., 2015). Here we found that TOB1 is capable of transporting IBA and nitrate, but not other tested hormones.

This transport is electrogenic and TOB1 likely functions as a proton cotransporter, which either transports the anionic form of IBA with two protons or the protonated form with one proton (Figure 7B). Plant hormones are structurally diverse and arose at different points during the evolution of land plants. During evolution, flexibility within the NPF family allowed the transport of these hormone substrates. Of note, metazoan homologs appear to function as di- and tri-peptide transporters, but are well known to also transport a wide spectrum of drugs, supporting the hypothesis that the binding pocket is highly accommodating (Brandsch, 2013; Martinez Molledo et al., 2018). In addition to their hormone regulatory roles, the dual affinity of many of these transporters provides a mechanism to integrate nitrate and hormone-regulated growth (reviewed in Krouk, 2016).

Our biochemical experiments (Figure 2), root tip transport assays (Figure 2), and response assays to the inhibitory effects of IBA on root elongation (Figure 1) are consistent with proton-coupled IBA and nitrate efflux from the vacuole (Figure 7C) under high IBA concentrations. However, the affinity of TOB1 for IBA is apparently low (millimolar range) and the presence of nitrate in the vacuole is expected to affect IBA efflux. Analysis of *tob1* mutant developmental phenotypes (Figures 4 and 5), root tip transport assays (Figure 2), cytokinin response assays (Figure 6), localization (Figures 3 and S3), and yeast transport assays (Figure 2) support an *in planta* role of TOB1 in IBA transport into the vacuole (Figure 7C). However, our electrophysiology analysis (Figure 2) and localization data (Figures 3 and S3) are consistent with a role for TOB1 in moving IBA out of the vacuole (Figure 7C). These alternative models of TOB1 activity in the cell are each differentially supported by our data and no one model can explain our current data, suggesting that there are additional factors at play and/or that TOB1 functions differently in distinct cell types. Thus, we hypothesize that other factors affect the transport efficacy and selectivity of this protein *in vivo*. For example, the high-affinity nitrate transporters of the NRT2 family require a second subunit, NAR2 for activity (Okamoto et al., 2006; Yong et al., 2010). It is possible that NPF proteins similarly interact with regulators that affect the direction, selectivity, and capacity to transport diverse plant hormones.

Our studies have uncovered a previously unknown protein with roles in the regulation of lateral root development that integrates cytokinin responses and modulation of auxin levels through controlling IBA inputs into the auxin pool (Figure 6). Lateral root branching is instrumental in shaping root system architecture, which in turn drives belowground resource acquisition (reviewed in Lavenus et al., 2013). Mutants defective in TOB1 more thoroughly explore within the volume of space they occupy, which may be advantageous in certain environments. Because *TOB1* expression is dynamically controlled by cytokinin, TOB1 may serve as a rheostat for modulating auxin levels in specific tissues to ultimately affect the final root architecture. It will be interesting in the future to determine whether TOB1 is involved in the root system architecture changes associated with nutrient availability and stress responses.

STAR★METHODS

Detailed methods are provided in the online version of this paper and include the following:

- KEY RESOURCES TABLE
- LEAD CONTACT AND MATERIALS AVAILABILITY
- EXPERIMENTAL MODEL AND SUBJECT DETAILS
  - Arabidopsis
- METHOD DETAILS
  - Growth Conditions and Phenotypic Assays
  - Genetic Analysis
  - Vector Construction and Transformation
  - Root System Architecture Analysis
  - Microscopy
  - Auxin Accumulation Assays
  - RNA Isolation and qPCR
- QUANTIFICATION AND STATISTICAL ANALYSIS

SUPPLEMENTAL INFORMATION

Supplemental Information can be found online at https://doi.org/10.1016/j.devcel.2019.06.010.

ACKNOWLEDGMENTS

We would like to thank the ABRC for providing *TOB1* cDNA and Ryan Emenecker, Hongwei Jing, and Nick Morffy for critical comments on the manuscript. We thank the Genome Technology Access Center in the Department of Genetics at Washington University School of Medicine for help with genomic analysis. The Center is partially supported by the National Cancer Institute Cancer Center Support grant (P30 CA91842) to the Siteman Cancer Center and by ITCTS/CTSA (UL1 TR000448) from the National Center for Research Resources, a component of the National Institutes of Health (NIH), and the NIH Roadmap for Medical Research. This research was supported by the William H. Danforth Plant Science Fellowship Program (to S.K.P.), the National Science Foundation (DGE-1143954 to T.A.E., IIA-1355406 and IOS-1638507 to C.N.T., MCB-1413254 to W.F., and IOS-1453750 to L.C.S.), the NSF Center for Engineering Mechanobiology (CMMI-1548571 to L.C.S.), the National Institutes of Health (R01 GM112898 to L.C.S.), an Alexander von Humboldt Professorship (to W.F.), Academia Sinica (C.-H.H.), and the Ministry of Science and Technology, Taiwan (106-2311-B-001 -037 -MY3 to C.-H.H.).

AUTHOR CONTRIBUTIONS

Conceptualization, M.P. and L.C.S.; Methodology, E.F. and C.N.T.; Investigation, M.P., T.A.E., C.-H.H., T.A.E., E.F., L.K.G., S.D., S.K.P., E.M.F., and L.C.S.; Resources, C.N.T and W.B.F.; Writing, M.P. and L.C.S.; Supervision, C.N.T., W.B.F., and L.C.S.

DECLARATION OF INTERESTS

The authors declare no competing interests.

Received: February 12, 2019
Revised: May 29, 2019
Accepted: June 14, 2019
Published: July 18, 2019

REFERENCES

Bielach, A., Podlesakova, K., Marhavy, P., Duclercq, J., Cuesta, C., Muller, B., Grunewald, W., Tarkowski, P., and Benkova, E. (2012). Spatiotemporal regulation of lateral root organogenesis in Arabidopsis by cytokinin. Plant Cell *24*, 3967–3981.

Brandsch, M. (2013). Drug transport via the intestinal peptide transporter PepT1. Curr. Opin. Pharmacol. *13*, 881–887.

Casimiro, I., Beeckman, T., Graham, N., Bhalerao, R., Zhang, H., Casero, P., Sandberg, G., and Bennett, M.J. (2003). Dissecting *Arabidopsis* lateral root development. Trends Plant Sci. *8*, 165–171.

Chandler, J.W., and Werr, W. (2015). Cytokinin-auxin crosstalk in cell type specification. Trends Plant Sci. *20*, 291–300.

Chang, L., Ramireddy, E., and Schmulling, T. (2013). Lateral root formation and growth of Arabidopsis is redundantly regulated by cytokinin metabolism and signalling genes. J. Exp. Bot. *64*, 5021–5032.

Chiba, Y., Shimizu, T., Miyakawa, S., Kanno, Y., Koshiba, T., Kamiya, Y., and Seo, M. (2015). Identification of *Arabidopsis thaliana* NRT1/PTR FAMILY (NPF) proteins capable of transporting plant hormones. J. Plant Res. *128*, 679–686.

Cingolani, P., Platts, A., Wang, le L., Coon, M., Nguyen, T., Wang, L., Land, S.J., Lu, X., and Ruden, D.M. (2012). A program for annotating and predicting the effects of single nucleotide polymorphisms, SnpEff: SNPs in the genome of Drosophila melanogaster strain w1118; iso-2; iso-3. Fly (Austin) *6*, 80–92.

Clough, S.J., and Bent, A.F. (1998). Floral dip: a simplified method for *Agrobacterium*-mediated transformation of *Arabidopsis thaliana*. Plant J. *16*, 735–743.

De Michele, R., Ast, C., Loqué, D., Ho, C.H., Andrade, S.L., Lanquar, V., Grossmann, G., Gehne, S., Kumke, M.U., and Frommer, W.B. (2013). Fluorescent sensors reporting the activity of ammonium transceptors in live cells. ELife *2*, e00800.

De Rybel, B., Audenaert, D., Xuan, W., Overvoorde, P., Strader, L.C., Kepinski, S., Hoye, R., Brisbois, R., Parizot, B., Vanneste, S., et al. (2012). A role for the root cap in root branching revealed by the non-auxin probe naxillin. Nat. Chem. Biol. *8*, 798–805.

De Smet, I., Tetsumura, T., De Rybel, B., Frei dit Frey, N., Laplaze, L., Casimiro, I., Swarup, R., Naudts, M., Vanneste, S., Audenaert, D., et al. (2007). Auxin-dependent regulation of lateral root positioning in the basal meristem of Arabidopsis. Development *134*, 681–690.

Friml, J., Vieten, A., Sauer, M., Weijers, D., Schwarz, H., Hamann, T., Offringa, R., and Jürgens, G. (2003). Efflux-dependent auxin gradients establish the apical-basal axis of *Arabidopsis*. Nature *426*, 147–153.

Frommer, W.B., Hummel, S., and Rentsch, D. (1994). Cloning of an Arabidopsis histidine transporting protein related to nitrate and peptide transporters. FEBS Lett. *347*, 185–189.

Galkovskyi, T., Mileyko, Y., Bucksch, A., Moore, B., Symonova, O., Price, C.A., Topp, C.N., Iyer-Pascuzzi, A.S., Zurek, P.R., Fang, S., et al. (2012). GiA Roots: software for the high throughput analysis of plant root system architecture. BMC Plant Biol. *12*, 116.

Haughn, G.W., and Somerville, C. (1986). Sulfonylurea-resistant mutants of *Arabidopsis thaliana*. Mol. Gen. Genet. *204*, 430–434.

He, Y.N., Peng, J.S., Cai, Y., Liu, D.F., Guan, Y., Yi, H.Y., and Gong, J.M. (2017). Tonoplast-localized nitrate uptake transporters involved in vacuolar nitrate efflux and reallocation in Arabidopsis. Sci. Rep. *7*, 6417.

Ho, C.H., and Frommer, W.B. (2014). Fluorescent sensors for activity and regulation of the nitrate transceptor CHL1/NRT1.1 and oligopeptide transporters. ELife *3*, e01917.

Ho, C.H., Lin, S.H., Hu, H.C., and Tsay, Y.F. (2009). CHL1 functions as a nitrate sensor in plants. Cell *138*, 1184–1194.

Huang, N.C., Liu, K.H., Lo, H.J., and Tsay, Y.F. (1999). Cloning and functional characterization of an Arabidopsis nitrate transporter gene that encodes a constitutive component of low-affinity uptake. Plant Cell *11*, 1381–1392.

Ito, H., and Gray, W.M. (2006). A gain-of-function mutation in the Arabidopsis pleiotropic drug resistance transporter PDR9 confers resistance to auxinic herbicides. Plant Physiol. *142*, 63–74.

Kanno, Y., Hanada, A., Chiba, Y., Ichikawa, T., Nakazawa, M., Matsui, M., Koshiba, T., Kamiya, Y., and Seo, M. (2012). Identification of an abscisic acid transporter by functional screening using the receptor complex as a sensor. Proc. Natl. Acad. Sci. USA *109*, 9653–9658.

Koncz, C., and Schell, J. (1986). The promoter of the T_L-DNA gene 5 controls the tissue-specific expression of chimaeric genes carried by a novel type of *Agrobacterium* binary vector. Mol. Gen. Genet. *204*, 383–396.

Krouk, G. (2016). Hormones and nitrate: a two-way connection. Plant Mol. Biol. *91*, 599–606.

Krouk, G., Lacombe, B., Bielach, A., Perrine-Walker, F., Malinska, K., Mounier, E., Hoyerova, K., Tillard, P., Leon, S., Ljung, K., et al. (2010). Nitrate-regulated auxin transport by NRT1.1 defines a mechanism for nutrient sensing in plants. Dev. Cell *18*, 927–937.

Laplaze, L., Benkova, E., Casimiro, I., Maes, L., Vanneste, S., Swarup, R., Weijers, D., Calvo, V., Parizot, B., Herrera-Rodriguez, M.B., et al. (2007). Cytokinins act directly on lateral root founder cells to inhibit root initiation. Plant Cell *19*, 3889–3900.

Last, R.L., and Fink, G.R. (1988). Tryptophan-requiring mutants of the plant *Arabidopsis thaliana*. Science *240*, 305–310.

Lavenus, J., Goh, T., Roberts, I., Guyomarc'h, S., Lucas, M., De Smet, I., Fukaki, H., Beeckman, T., Bennett, M., and Laplaze, L. (2013). Lateral root development in Arabidopsis: fifty shades of auxin. Trends Plant Sci. *18*, 450–458.

Leisgen, C., Kuester, M., and Methfessel, C. (2007). The roboocyte: automated electrophysiology based on Xenopus oocytes. Methods Mol. Biol. *403*, 87–109.

Léran, S., Varala, K., Boyer, J.C., Chiurazzi, M., Crawford, N., Daniel-Vedele, F., David, L., Dickstein, R., Fernandez, E., Forde, B., et al. (2014). A unified nomenclature of NITRATE Transporter 1/PEPTIDE Transporter family members in plants. Trends Plant Sci. *19*, 5–9.

Li, B., Byrt, C., Qiu, J., Baumann, U., Hrmova, M., Evrard, A., Johnson, A.A., Birnbaum, K.D., Mayo, G.M., Jha, D., et al. (2016). Identification of a stelar-localized transport protein that facilitates root-to-shoot transfer of chloride in Arabidopsis. Plant Physiol. *170*, 1014–1029.

Li, H., Handsaker, B., Wysoker, A., Fennell, T., Ruan, J., Homer, N., Marth, G., Abecasis, G., and Durbin, R.; 1000 Genome Project Data Processing Subgroup (2009). The Sequence Alignment/Map format and SAMtools. Bioinformatics *25*, 2078–2079.

Loqué, D., Mora, S.I., Andrade, S.L., Pantoja, O., and Frommer, W.B. (2009). Pore mutations in ammonium transporter AMT1 with increased electrogenic ammonium transport activity. J. Biol. Chem. *284*, 24988–24995.

Lynch, J.P., Ho, M.D., and phosphorus, L. (2005). Rhizoeconomics: carbon costs of phosphorus acquisition. Plant Soil *269*, 45–56.

Malamy, J.E., and Benfey, P.N. (1997). Organization and cell differentiation in lateral roots of *Arabidopsis thaliana*. Development *124*, 33–44.

Marhavý, P., Bielach, A., Abas, L., Abuzeineh, A., Duclercq, J., Tanaka, H., Parezová, M., Petrášek, J., Friml, J., Kleine-Vehn, J., et al. (2011). Cytokinin modulates endocytic trafficking of PIN1 auxin efflux carrier to control plant organogenesis. Dev. Cell *21*, 796–804.

Marhavý, P., Duclercq, J., Weller, B., Feraru, E., Bielach, A., Offringa, R., Friml, J., Schwechheimer, C., Murphy, A., and Benková, E. (2014). Cytokinin controls polarity of PIN1-dependent auxin transport during lateral root organogenesis. Curr. Biol. *24*, 1031–1037.

Martinez Molledo, M., Quistgaard, E.M., Flayhan, A., Pieprzyk, J., and Löw, C. (2018). Multispecific substrate recognition in a proton-dependent oligopeptide transporter. Structure *26*, 467–476.

Michniewicz, M., Frick, E.M., and Strader, L.C. (2015). Gateway-compatible tissue-specific vectors for plant transformation. BMC Res. Notes *8*, 63.

Michniewicz, M., Powers, S.K., and Strader, L.C. (2014). IBA transport by PDR proteins. In Plant ABC transporters, M. Geisler, ed. (Springer International Publishing), pp. 313–331.

Moreira, S., Bishopp, A., Carvalho, H., and Campilho, A. (2013). AHP6 inhibits cytokinin signaling to regulate the orientation of pericycle cell division during lateral root initiation. PLoS One *8*, e56370.

Moreno-Risueno, M.A., Van Norman, J.M., Moreno, A., Zhang, J., Ahnert, S.E., and Benfey, P.N. (2010). Oscillating gene expression determines competence for periodic Arabidopsis root branching. Science *329*, 1306–1311.

Mounier, E., Pervent, M., Ljung, K., Gojon, A., and Nacry, P. (2014). Auxin-mediated nitrate signalling by NRT1.1 participates in the adaptive response of Arabidopsis root architecture to the spatial heterogeneity of nitrate availability. Plant Cell Environ. *37*, 162–174.

Nishimura, C., Ohashi, Y., Sato, S., Kato, T., Tabata, S., and Ueguchi, C. (2004). Histidine kinase homologs that act as cytokinin receptors possess overlapping functions in the regulation of shoot and root growth in Arabidopsis. Plant Cell *16*, 1365–1377.

Nour-Eldin, H.H., Andersen, T.G., Burow, M., Madsen, S.R., Jørgensen, M.E., Olsen, C.E., Dreyer, I., Hedrich, R., Geiger, D., and Halkier, B.A. (2012). NRT/PTR transporters are essential for translocation of glucosinolate defence compounds to seeds. Nature *488*, 531–534.

Okamoto, M., Kumar, A., Li, W., Wang, Y., Siddiqi, M.Y., Crawford, N.M., and Glass, A.D. (2006). High-affinity nitrate transport in roots of Arabidopsis depends on expression of the NAR2-like gene *AtNRT3.1*. Plant Physiol. *140*, 1036–1046.

Pehl, U., Leisgen, C., Gampe, K., and Guenther, E. (2004). Automated higher-throughput compound screening on ion channel targets based on the Xenopus laevis oocyte expression system. Assay Drug Dev. Technol. *2*, 515–524.

Pfaffl, M.W. (2001). A new mathematical model for relative quantification in real-time RT-PCR. Nucleic Acids Res. *29*, e45.

Rentsch, D., Laloi, M., Rouhara, I., Schmelzer, E., Delrot, S., and Frommer, W.B. (1995). NTR1 encodes a high affinity oligopeptide transporter in Arabidopsis. FEBS Lett. *370*, 264–268.

Rogers, E.D., and Benfey, P.N. (2015). Regulation of plant root system architecture: implications for crop advancement. Curr. Opin. Biotechnol. *32*, 93–98.

Sabatini, S., Beis, D., Wolkenfelt, H., Murfett, J., Guilfoyle, T., Malamy, J., Benfey, P., Leyser, O., Bechtold, N., Weisbeek, P., and Scheres, B. (1999). An auxin-dependent distal organizer of pattern and polarity in the Arabidopsis root. Cell *99*, 463–472.

Saito, H., Oikawa, T., Hamamoto, S., Ishimaru, Y., Kanamori-Sato, M., Sasaki-Sekimoto, Y., Utsumi, T., Chen, J., Kanno, Y., Masuda, S., et al. (2015). The jasmonate-responsive GTR1 transporter is required for gibberellin-mediated stamen development in Arabidopsis. Nat. Commun. *6*, 6095.

Satbhai, S.B., Ristova, D., and Busch, W. (2015). Underground tuning: quantitative regulation of root growth. J. Exp. Bot. *66*, 1099–1112.

Schaller, G.E., Bishopp, A., and Kieber, J.J. (2015). The yin-yang of hormones: cytokinin and auxin interactions in plant development. Plant Cell *27*, 44–63.

Schwacke, R., Schneider, A., van der Graaff, E., Fischer, K., Catoni, E., Desimone, M., Frommer, W.B., Flügge, U.I., and Kunze, R. (2003). ARAMEMNON, a novel database for Arabidopsis integral membrane proteins. Plant Physiol. *131*, 16–26.

Šimášková, M., O'Brien, J.A., Khan, M., Van Noorden, G., Ötvös, K., Vieten, A., De Clercq, I., Van Haperen, J.M.A., Cuesta, C., Hoyerová, K., et al. (2015). Cytokinin response factors regulate PIN-FORMED auxin transporters. Nat. Commun. *6*, 8717.

Stasinopoulos, T.C., and Hangarter, R.P. (1990). Preventing photochemistry in culture media by long-pass light filters alters growth of cultured tissues. Plant Physiol. *93*, 1365–1369.

Stein, M., Dittgen, J., Sánchez-Rodríguez, C., Hou, B.H., Molina, A., Schulze-Lefert, P., Lipka, V., and Somerville, S. (2006). Arabidopsis PEN3/PDR8, an ATP binding cassette transporter, contributes to nonhost resistance to inappropriate pathogens that enter by direct penetration. Plant Cell *18*, 731–746.

Strader, L.C., and Bartel, B. (2009). The Arabidopsis PLEIOTROPIC DRUG RESISTANCE8/ABCG36 ATP binding cassette transporter modulates sensitivity to the auxin precursor indole-3-butyric acid. Plant Cell *21*, 1992–2007.

Strader, L.C., and Bartel, B. (2011). Transport and metabolism of the endogenous auxin precursor indole-3-butyric acid. Mol. Plant *4*, 477–486.

Strader, L.C., Monroe-Augustus, M., Rogers, K.C., Lin, G.L., and Bartel, B. (2008). Arabidopsis *iba response5 (ibr5)* suppressors separate responses to various hormones. Genetics *180*, 2019–2031.

Strader, L.C., Wheeler, D.L., Christensen, S.E., Berens, J.C., Cohen, J.D., Rampey, R.A., and Bartel, B. (2011). Multiple facets of *Arabidopsis* seedling development require indole-3-butyric acid-derived auxin. Plant Cell *23*, 984–999.

Symonova, O., Topp, C.N., and Edelsbrunner, H. (2015). DynamicRoots: A software platform for the reconstruction and analysis of growing plant roots. PLoS One *10*, e0127657.

Taylor-Teeples, M., Lanctot, A., and Nemhauser, J.L. (2016). As Above, So Below: auxin's role in lateral organ development. Dev. Biol. *419*, 156–164.

Thole, J.M., Beisner, E.R., Liu, J., Venkova, S.V., and Strader, L.C. (2014). Abscisic acid regulates root elongation through the activities of auxin and ethylene in *Arabidopsis thaliana*. G3 (Bethesda) *4*, 1259–1274.

Thole, J.M., and Strader, L.C. (2015). Next-generation sequencing as a tool to quickly identify causative EMS-generated mutations. Plant Signal. Behav. *10*, e1000167.

Topp, C.N., Iyer-Pascuzzi, A.S., Anderson, J.T., Lee, C.R., Zurek, P.R., Symonova, O., Zheng, Y., Bucksch, A., Mileyko, Y., Galkovskyi, T., et al. (2013). 3D phenotyping and quantitative trait locus mapping identify core regions of the rice genome controlling root architecture. Proc. Natl. Acad. Sci. USA *110*, E1695–E1704.

Tsay, Y.F., Schroeder, J.I., Feldmann, K.A., and Crawford, N.M. (1993). The herbicide sensitivity gene *CHL1* of Arabidopsis encodes a nitrate-inducible nitrate transporter. Cell *72*, 705–713.

Xuan, W., Audenaert, D., Parizot, B., Möller, B.K., Njo, M.F., De Rybel, B., De Rop, G., Van Isterdael, G., Mähönen, A.P., Vanneste, S., et al. (2015). Root cap-derived auxin pre-patterns the longitudinal axis of the Arabidopsis Root. Curr. Biol. *25*, 1381–1388.

Xuan, W., Band, L.R., Kumpf, R.P., Van Damme, D., Parizot, B., De Rop, G., Opdenacker, D., Möller, B.K., Skorzinski, N., Njo, M.F., et al. (2016). Cyclic programmed cell death stimulates hormone signaling and root development in Arabidopsis. Science *351*, 384–387.

Yong, Z., Kotur, Z., and Glass, A.D. (2010). Characterization of an intact two-component high-affinity nitrate transporter from Arabidopsis roots. Plant J. *63*, 739–748.

Zhang, W., To, J.P., Cheng, C.Y., Schaller, G.E., and Kieber, J.J. (2011). Type-A response regulators are required for proper root apical meristem function through post-transcriptional regulation of PIN auxin efflux carriers. Plant J. *68*, 1–10.

Zhou, J.J., Theodoulou, F.L., Muldin, I., Ingemarsson, B., and Miller, A.J. (1998). Cloning and functional characterization of a *Brassica napus* transporter that is able to transport nitrate and histidine. J. Biol. Chem. *273*, 12017–12023.

Zolman, B.K., Martinez, N., Millius, A., Adham, A.R., and Bartel, B. (2008). Identification and characterization of *Arabidopsis* indole-3-butyric acid response mutants defective in novel peroxisomal enzymes. Genetics *180*, 237–251.

Zolman, B.K., Yoder, A., and Bartel, B. (2000). Genetic analysis of indole-3-butyric acid responses in *Arabidopsis thaliana* reveals four mutant classes. Genetics *156*, 1323–1337.

Zubo, Y.O., Blakley, I.C., Yamburenko, M.V., Worthen, J.M., Street, I., Franco-Zorrilla, J.M., Zhang, W., Hill, K., Raines, T., Solano, R., et al. (2017). Cytokinin induces genome-wide binding of the type-B response regulator ARR10 to regulate growth and development in Arabidopsis. Proc Natl Acad Sci USA *114*, E5995–E6004.

STAR★METHODS

KEY RESOURCES TABLE

REAGENT or RESOURCE	SOURCE	IDENTIFIER
Chemicals, Peptides, and Recombinant Proteins		
Indole-3-Butyric Acid (IBA)	Sigma-Aldrich	I5386
Indole-3-Acetic Acid (IAA)	Sigma-Aldrich	I2886
Basta	GoldBio	P-165-1
Kinetin	Sigma-Aldrich	K3378
6-Benzylaminopurine (BA)	Sigma-Aldrich	B3408
[3H]IBA	American Radiolabeled Chemicals	ART1112
[3H]IAA	American Radiolabeled Chemicals	ART0340
Ethyl-methansulfonate (EMS)	Sigma-Aldrich	M0880
Critical Commercial Assays		
RNeasy Plant Mini Kit	Qiagen	74904
QuikChange Lightning Multi Site-Directed Mutagenesis Kit	Agilent	210518
mMESSAGE mMACHINE	Ambion	AM1340
iTaq Universal SYBR Green Supermix	Biorad	1725121
Experimental Models: Organisms/Strains		
Arabidopsis: pen3–4	Stein et al., 2006	N/A
Arabidopsis: pen3–4 tob1-1 (PS173)	this study	N/A
Arabidopsis: tob1-2	this study	SALK_093015
Arabidopsis: tob1-3	this study	SALK_205450
Arabidopsis: ech2-1 ibr10-1	Strader et al., 2011	N/A
Arabidopsis: tob1-1 ech2-1 ibr10-1	this study	N/A
Arabidopsis: tob1-1 pTOB1:YFP-TOB1	this study	N/A
Arabidopsis: DR5-GFP	Sabatini et al., 1999	N/A
Saccharomyces: pAG424-GFP	this study	N/A
Saccharomyces: pAG424-GFP-TOB1	this study	N/A
Arabidopsis: ahk3,4	Nishimura et al., 2004	
Arabidopsis: arr3,4,5,6,7,8,9,15	Zhang et al., 2011	
Oligonucleotides		
GCTGTGTTGAGTCTCATTCC	this study	TOB1-Fmut
CTCGACCAAAGCAGCTATTACC	this study	TOB1-Rmut
GCATGGATGGGAGATCGGCCG	this study	TOB1-2-F
GCCTAAGATCCAACTCATGCC	this study	TOB1-2-R
CAAACCAGCGTGGACCGCTTGCTGCAACTC	this study	LB1-SALK
CGTGAGTCGTGCGTCTCTCAGG	this study	TOB1-3-F
GATTGATCGTGCGATTGGGACG	this study	TOB1-3-R
GAATTCGCGATACACTGAGACTAACGC	this study	promTOB1-F
CTCGAGGCTTCTTGTTATTTCGTTTCAG	this study	promTOB1-R
CACCATGTCGACATCCATCGGCGAT	this study	TOB1cDNA-F
CTACTTTGGGCTGTTGTAGAGATAG	this study	TOB1cDNA-R
AAAGAGAAGGAATCGTTGCTGAAA	this study	TOB1-10
CTTCACCGAGGCGTTAGGAGAGTC	this study	TOB1-11
TTCCGTACCCTCAAGCTCGCTAAT	this study	bTUB-F2
ATCCTCTCGATGTCAATGGTGCGA	this study	bTUB-R2

(*Continued on next page*)

Continued		
REAGENT or RESOURCE	SOURCE	IDENTIFIER
Recombinant DNA		
pMCS:YFP-GW	Michniewicz et al., 2015	ABRC stock #CD3-1934
cDNA U66577 (TOB1)	Arabidopsis Biological Resource Center (ABRC)	N/A
pOO2-GW	Loqué et al., 2009	N/A
pOO2-TOB1	this study	N/A
pOO2-TOB1D457A	this study	N/A
Software and Algorithms		
ImageJ	NIH	https://imagej.nih.gov/ij/
Novoalign	Novocraft	http://novocraft.com
SAMtools	Li et al., 2009	N/A
snpEFF	Cingolani et al., 2012	N/A
RSA-Gia	Galkovskyi et al., 2012; Topp et al., 2013	N/A
Dynamic Roots	Symonova et al., 2015	N/A

LEAD CONTACT AND MATERIALS AVAILABILITY

Further information and requests for resources and reagents should be directed to and will be fulfilled by the Lead Contact, Lucia Strader (strader@wustl.edu).

EXPERIMENTAL MODEL AND SUBJECT DETAILS

Arabidopsis

All *Arabidopsis* lines were in the Columbia (Col-0) background, which was used as the wild type (WT). Seeds were surface-sterilized (Last and Fink, 1988), suspended in 0.1% agar, and stratified for 2 d at 4°C to promote uniform germination. After stratification, seeds were plated on plant nutrient (PN) media (Haughn and Somerville, 1986) solidified with 0.6% agar and supplemented with 0.5% (w/v) sucrose (PNS) at 22°C under continuous illumination.

METHOD DETAILS

Growth Conditions and Phenotypic Assays

All plant lines were in the Columbia (Col-0) accession of *Arabidopsis thaliana*. Surface-sterilized (Last and Fink, 1988) seeds were plated on plant nutrient (PN, Haughn and Somerville, 1986) medium supplemented with 0.5% (w/v) sucrose and solidified with 0.6% (w/v) agar. Hormone stocks were dissolved in ethanol prior to supplementation of media for growth assays. Ethanol-supplemented media (Mock) were used as controls. Seedlings were grown at 22°C under continuous illumination through yellow long-pass filters to slow indolic compound breakdown (Stasinopoulos and Hangarter, 1990).

For auxin-responsive root elongation assays, primary root lengths of seedlings grown for the indicated number of days on media supplemented with the indicated auxin were imaged or manually measured.

For lateral root assays, seedlings were grown on unsupplemented medium or medium supplemented with the indicated hormone. Emerged lateral roots, as seen under a dissecting microscope, were counted. To quantify lateral primordia, seedlings carrying the DR5:GFP reporter (Friml et al., 2003) were examined at the indicated time points using a Leica Axioimager and lateral root primordia staged according to Malamy and Benfey (1997).

For cytokinin-responsive root elongation assays, primary root lengths of seedlings grown for 10 days on media supplemented with ethanol (Mock) or 0.5 μM kinetin were measured. For cytokinin-responsive lateral root assays, emerged lateral roots were counted and primary root lengths of seedlings grown for 10 days on media supplemented with ethanol (Mock) or 0.5 μM kinetin were measured. For each seedling, the number of emerged lateral roots was divided by the primary root length to determine lateral root density.

Genetic Analysis

Seeds of the *pen3-4* (Stein et al., 2006) mutant were mutagenized by treatment with 0.24% ethyl-methansulfonate (EMS) for 16 h. These M_1 seed were moved to soil and allowed to self-fertilize. The resultant M_2 seed were surface-sterilized and plated on media supplemented with 10 μM IBA. Seedlings displaying suppressed *pen3-4* hypersensitivity to IBA (Strader and Bartel, 2009) were selected, given a “PS” designation number, moved to soil, and allowed to self-fertilize. M_3 progeny were retested for suppression of *pen3-4* IBA and 2,4-DB hypersensitivity (Figure S1). Those individuals that passed the retest for suppression of *pen3-4* hypersensitivity to the auxin precursors IBA and 2,4-DB were then tested for sensitivity to the active auxins IAA and dichlorophenoxyacetic acid (2,4-D) Isolates displaying resistance to these active auxins were discarded. Remaining isolates displaying a requirement for a fixed carbon source to fuel growth were eliminated because they were likely defective in generic peroxisomal processes (Zolman et al., 2000), rather than processes specific to the auxin precursor IBA. From the remaining isolates, we focused on those displaying suppression of *pen3-4* hyperaccumulation of the [^{3}H]-IBA in root tip auxin accumulation assays (Strader and Bartel, 2009). *pen3-4* suppressor isolates PS1, PS88, PS89, PS142, PS173, PS200, and PS217 displayed suppressed the IBA and 2,4-DB hypersensitivity and suppressed the [^{3}H]IBA hyperaccumulation observed in *pen3-4* (Figure S1).

The causative mutation in PS173 was identified by a bulk segregant whole genome sequencing strategy (Thole and Strader, 2015). PS173 was crossed to *pen3-4* and resultant F_2 progeny were selected for suppression of IBA hypersensitivity (Figure S1C), moved to soil, and allowed to self-fertilize. Seedlings from F_3 progeny that retested for suppression of IBA hypersensitivity were combined for genomic DNA extraction (Thole et al., 2014). Genomic library preparation, Illumina sequencing, and data analysis were performed as previously described (Thole et al., 2014).

PCR-based assays were used to verify genotypes. Amplification of *TOB1* with TOB1-Fmut (5'- GCTGTGTTGAGTCTCATTCC -3') and TOB1-Rmut (5'- CTCGACCAAAGCAGCTATTACC -3') results in a 316-bp product with three *Mnl*I sites in wild type and two sites in *tob1-1*. Amplification of *TOB1* with TOB1-2-F (5'- GCATGGATGGGAGATCGGCCG -3') and TOB1-2-R (5'- GCCTAAGATCCAACT CATGCC -3') results in an 870-bp product in wild type and no product in *tob1-2*. PCR amplification with TOB1-2-R and LB1-SALK (5'- CAAACCAGCGTGGACCGCTTGCTGCAACTC -3') results in an ~400-bp product in *tob1-2* and no product in wild type. Amplification of *TOB1* with TOB1-3-F (5'- CGTGAGTCGTGCGTCTCTCAGG -3') and TOB1-3-R (5'- GATTGATCGTGCGATTGGGACG -3') results in a 1077-bp product in wild type and no product in *tob1-3*. PCR amplification with TOB1-3-R and LB1-SALK results in an ~600-bp product in *tob1-3* and no product in wild type.

Vector Construction and Transformation

The *TOB1* upstream regulatory region was amplified using promTOB1-F (5'- GAATTCGCGATACACTGAGACTAACGC -3') and promTOB1-R (5'- CTCGAGGCTTCTTGTTATTTCGTTTCAG -3'). The resultant 1327-bp product, spanning the region between *TOB1* and its most upstream neighboring gene, was cloned into the pCR4 vector (Life Technologies) to create pCR4-TOB1prom. The *TOB1* upstream regulatory region was excised from pCR4-TOB1prom using *Eco*RI and *Xho*I and subcloned into pMCS:YFP-GW (Michniewicz et al., 2015) to create pTOB1:YFP-GW.

A *TOB1* cDNA was amplified from the U66577 clone obtained from the ABRC (Ohio State University) using Pfx Platinum Taq (Life Technologies) using TOB1cDNA-F (5'- CACCATGTCGACATCCATCGGCGAT -3') and TOB1cDNA-R (5'- CTACTTTGGGCTGTTG TAGAGATAG -3'). The resultant PCR product was captured into the pENTR/D-TOPO vector (Life Technologies) to give pENTR-TOB1c. This *TOB1* cDNA was recombined into the pTOB1:YFP-GW vector using LR Clonase (Life Technologies) to form pTOB1:YFP-TOB1, which expresses an N-terminal YFP fusion with TOB1 driven by the *TOB1* genomic upstream regulatory region. Recombinant plasmids were transformed into *Agrobacterium tumefaciens* strain GV3101 (Koncz and Schell, 1986), which was used to transform plants using the floral dip method (Clough and Bent, 1998). Transformants were selected in the presence of 10 μg/mL Basta (phosphinothricin) and lines homozygous for the transgene were identified in subsequent generations.

The *TOB1* and *TOB1*^{D457A} cDNAs were recombined into the pOO2-GW vector (Loqué et al., 2009) using LR Clonase (Life Technologies) to form pOO2-TOB1 and pOO2-TOB1^{D457A}, which allows for generation of *TOB1* and *TOB1*^{D457A} transcripts compatible with *Xenopus* oocyte translation.

Root System Architecture Analysis

Seeds (Col-0 and *tob1-1*) were vapor sterilized for 30 min with chlorine gas and then cold stratified in sterile H_2O for 48 h prior to being planted in 2 L glass cylinders containing 1.5 L of plant nutrient medium (PN, Haughn and Somerville, 1986) supplemented with 0.5% (w/v) sucrose solidified with 0.15% (w/v) gellan gum (Gelzan, Caisson Labs). Excess seeds were thinned from cylinders at 3 days-post-planting leaving one plant per cylinder. Plants were grown at 23°C for 14-hour days, and 21°C for 10-hour nights. Starting at 9 days-post-planting, plants were imaged on a custom optical projection tomography system every 4 days until they reached 25 days post planting. The details of this system are described in Topp et al. (2013), but in brief, the cylinders were placed on a backlit turntable controlled by a computer. As the cylinder spins across 360 degrees, a sillhouete image is captured every 5 degrees for a total of 72 images per data set. Images were scaled, cropped, and thresholded, prior to 3D reconstructions and global feature extractions using the RSA-Gia pipeline (Galkovskyi et al., 2012; Topp et al., 2013) (Data S1). Timeseries analysis of individual roots within the root system were conducted by exporting 3D models from the RSA-Gia pipeline into the Dynamic Roots application (Symonova et al., 2015) (Data S2).

Microscopy

Seedlings were mounted in water for imaging through a 40× water immersion lens on a Zeiss LSM 510 laser scanning microscope equipped with a Meta detector. Pixels resulting from fluorescence were false-colored yellow. Images were converted and channels merged using NIH ImageJ.

Auxin Accumulation Assays

Arabidopsis Root Tip Transport Assays

Auxin accumulation assays were performed as previously described on excised root tips from 8-day-old seedlings (Strader and Bartel, 2009), except that root tips were moved to scintillant immediately after being rinsed following incubation in radiolabeled auxin.

Saccharomyces cerevisiae Transport Assays

Saccharomyces cerevisiae strain BY4741 was transformed with either pAG424-GFP to express free GFP or with pAG424-GFP-TOB1 to express GFP-TOB1. Yeast were grown overnight in a 50 culture to OD_{600} = 0.4 in SC-Trp. Cells were harvested by centrifugation and resuspended to OD_{600} = 1.0 in 0.1 M 2-(N-morpholino)ethanesulfonic acid (MES) buffer (pH 4.6) supplemented with 2% glucose. 50 μl cells were aliquoted into an eppendorf tube and an equal volume of 50 nM [^{3}H]-IAA or 50 nM [^{3}H]-IBA added to each tube, for a final concentration of 25 nM [^{3}H]-IAA or 25 nM [^{3}H]-IBA. Cells were incubated at room temperature for 1 h, resuspended and rinsed three times with 0.1 M MES buffer (pH 4.6) supplemented with 2% glucose, then moved to scintillant.

Xenopus Oocyte Transport Assays

TEVC in oocytes was performed essentially as described previously (Ho and Frommer, 2014). To obtain capped cRNA for *Xenopus* oocyte injections, pOO2-TOB1 and pOO2-TOB1^{D457A} were linearized with *Mlu*I and transcribed *in vitro* by SP6 RNA polymerase using the mMESSAGE mMACHINE kit (Ambion, Austin, TX). *Xenopus laevis* oocytes were obtained from the laboratory of Miriam Goodman by manual surgery or ordered from Ecocyte Bio Science (Austin, TX). Oocytes were injected with 50 nL distilled water, 50 ng *TOB1* cRNA, or 50 ng *TOB1*^{D457A} cRNA (in 50 nL volume) using a Roboinjector (Multi Channel Systems, Reutlingen, Germany) (Ho and Frommer, 2014; Leisgen et al., 2007; Pehl et al., 2004). Cells were kept at 16°C for 2–4 days in ND96 buffer (96 mM NaCl, 2 mM KCl, 1.8 mM $CaCl_2$, 1 mM $MgCl_2$, 5 mM HEPES, pH 7.4) supplemented with gentamycin (50 μg/μl) before recording experiments. Recordings were typically performed at day three after cRNA injection.

Electrophysiological analyses of injected oocytes were performed as described previously (De Michele et al., 2013; De Michele et al., 2013; Huang et al., 1999). Reaction buffers used for recording current (I)-voltage (V) relationships or whole-cell currents from the injected *Xenopus* oocytes at a holding potential of −120 were (i) 230 mM mannitol, 0.3 mM $CaCl_2$, and 10 mM HEPES at the pH indicated plus indicated concentrations of IBA or $CsNO_3$. Typical resting potentials were −40 mV. For determination of IV relationships, measurements were recorded in oocytes that were voltage clamped at −20 mV and a step protocol was used (20 to −200 mV for 300 ms, in −20 mV increments) and measured by the two-electrode voltage-clamp (TEVC) Roboocyte system (Multi Channel Systems) (Ho and Frommer, 2014; Leisgen et al., 2007; Pehl et al., 2004). A subset of experiments was carried out using a chloride-free buffer.

Isotopic nitrate uptake assays were performed using ^{15}N-labeled nitrate (Ho et al., 2009). Oocytes were injected with *TOB1* cRNA, *TOB1*^{D457A} cRNA, or water (control) and incubated at 16°C for 2–4 days in ND96 supplemented with gentamycin. For isotopic nitrate uptake assays, the oocytes were then incubated for 60-90 min in the indicated $^{15}NO_3^-$ medium containing 230 mM mannitol, 0.3 mM $CaCl_2$, 10 mM HEPES pH 5.5. After incubation, oocytes were rinsed five times with ND96 buffer and individually dried at 80°C for 1–2 days. ^{15}N content was analyzed in an ECS 4010 Elemental Combustion System (Costech Analytical Technologies) whose output was connected to a Delta plus Advantage mass spectrometer (Thermo Fisher Scientific).

RNA Isolation and qPCR

Ten 6-day-old seedlings were incubated at room temperature in mock treatment or in 10 μM 6-benzylaminopurine (BA; dissolved in KOH) for 1 h. Seedlings were then harvested and total RNA extracted using an RNeasy kit (Qiagen) according to manufacturer's instructions. cDNA was synthesized from equal amounts of total RNA from each sample using Superscript III (Life Technologies). Resultant cDNA was diluted 1:10 in 10 mM Tris, pH 8.0, for use in qPCR using a Bio-Rad CFX Connect Real-Time PCR system. For quantitative PCR reactions, 2 μL of the 1:10 cDNA was used as the template, along with final primer concentrations of 200 nM, and a 0.5X final reaction volume of iTaq Universal SYBR Green Supermix (BioRad). Relative *TOB1* transcript accumulation were analyzed using primers TOB1-10 (5'- AAAGAGAAGGAATCGTTGCTGAAA -3') and TOB1-11 (5'- CTTCACCGAGGCGTTAGGA GAGTC -3'). *TUB4* (*At5g44340*) transcript levels were used as a control and were analyzed using primers bTUB-F2 (5'- TTCCGTACCCTCAAGCTCGCTAAT -3') and bTUB-R2 (5'- ATCCTCTCGATGTCAATGGTGCGA -3'). The PCR cycle conditions consisted of a 5 min initial denaturation at 95°C, followed by 40 cycles of melting (95°C for 10 seconds) and annealing/extension a (56°C for 40 seconds). PCR products were then analyzed using a melt curve analysis. An efficiency calibrated model (Pfaffl, 2001) was used to analyze the data. Data represent the average of 3 biological replicates, each with themselves the average of 3 technical replicates per biological replicate.

QUANTIFICATION AND STATISTICAL ANALYSIS

Details of statistical analyses can be found in the figure legends. Microsoft Excel was used to perform statistical analyses for phenotypic assays. All error bars represent standard error of the mean.